An n-sided polygonal smoothed finite element method (nSFEM) for solid mechanics

K.Y. Dai[a,b,*], G.R. Liu[a,b], T.T. Nguyen[a]

[a]Center for Advanced Computations in Engineering Science (ACES), Department of Mechanical Engineering, National University of Singapore, 10 Kent Ridge Crescent 119260, Singapore

[b]Singapore-MIT Alliance (SMA), E4-04-10, 4 Engineering Drive 3, Singapore 117576, Singapore

Abstract

Smoothed finite element method (SFEM) using quadrilateral elements was recently proposed by Liu et al. [A smoothed finite element method for mechanics problems, Comput. Mech. 39 (2007) 859–877; Free and forced vibration analysis using the smoothed finite element method (SFEM), J. Sound Vib. 301 (2007) 803–820; Theoretical aspects of the smoothed finite element method (SFEM), Int. J. Numer. Methods Eng. (2006), in press] to improve the accuracy and convergence rate of the existing standard four-node finite element method (FEM). In this paper the SFEM is further extended to a more general case, n-sided polygonal smoothed finite elements (nSFEM), in which the problem domain can be discretized by a set of polygons, each with an arbitrary number of sides. Stability condition is examined for this type of new elements and some criteria are provided to avoid the presence of spurious zero-energy modes. Approach to constructing nSFEM shape functions are also suggested with emphasis on a novel and simple averaging method. Selective integration scheme is recommended to overcome volumetric locking for nearly incompressible materials. Several numerical examples are investigated and the present results are in good agreement with exact solutions or FEM results. It is found that the present method gives very accurate stresses and desirable convergence rate as compared with FEM. In addition problem domain can be discretized in a very flexible manner as demonstrated in the examples.
© 2007 Elsevier B.V. All rights reserved.

Keywords: Finite element method; Smoothed finite element method; Strain smoothing; Stability; Locking

1. Introduction

The finite element method (FEM) [1,2] has become the most popular and powerful numerical tool for solving problems in engineering and science. However, this does not mean that no improvement can be made on the current FEM. Recently smoothed finite element method (SFEM) has been proposed by Liu et al. [3,4] by means of combining the strain smoothing technique with the conventional FEM technology. In this method, strain smoothing operation is performed on an entire or part of an element to replace the conventional strains obtained using displacement-compatible equations in FEM. In SFEM both

approximated accuracy and convergence rate can be improved further while the number of variables remains unchanged as that of irreducible form. In addition, the SFEM has some other superior features. Due to the presence of strain projection process, only shape function itself is involved in the calculation of field gradients and no coordinate transformations need to be performed. Hence shape function used in the field approximation can be easily constructed and the element is allowed to be of arbitrary shape and thus field domain can be discretized in a more flexible way. Most importantly, these good features are gained without increasing the efforts in both modeling and computation and modification to existing FEM codes is also an easy task.

Later on they have also proved that the upper and lower bound solutions in SFEM can be obtained by varying the number of smoothing cells (SCs) that an element is divided [5]. If each element is employed as one cell, an upper bound solution

---

* Corresponding author. Singapore-MIT Alliance (SMA), E4-04-10, 4 Engineering Drive 3, Singapore 117576, Singapore. Tel.: +65 6516 4796; fax: +65 6775 2920.

E-mail address: smadky@nus.edu.sg (K.Y. Dai).

is retrieved that corresponds to finite element displacement-compatible model solution using reduced integration. Conversely if the number of SCs approaches infinity a lower bound solution can be obtained that conforms to the finite element displacement-compatible model using full integration. Generally the SFEM solution falls between the two bound solutions and with the increase of SC in a monotonic manner, the accuracy as well as the convergence rate will transform gradually from the upper bound to the lower bound [5]. With such a solid theoretical foundation established, users can therefore have more freedom in choosing a suitable number of SCs that gives desired accuracy.

However, some problems still remain unclear. As mentioned in [3], singularity problem often occurs in the process of computation if insufficient number of SCs is adopted in SFEM and as a result even single-element patch test can fail. We are still not clear about what is a suitable number of cells in the subdivision of an element with arbitrary number of sides. As any shape of quadrilateral element is workable in practice, can we use more general polygons (with arbitrary number of sides) for domain discretization? Will this type of element be stable and convergent and under what conditions? With these problems in mind we aim to extend the SFEM to even more general case, i.e., a smoothed polygonal element with arbitrary sides (or nSFEM). We try to find the answers by means of the existing theories and numerical approach in this work.

The paper is organized as follows. Section 2 will revisit the idea, formulation and theoretical aspects of SFEM briefly. Stability condition will be studied in detail in Section 3 and some

criteria will be given in selection of SCs. Some approaches will be suggested on the construction of shape functions for polygonal elements in Section 4. Some numerical examples will be analyzed to demonstrate the accuracy, stability and convergence properties of the present method in Section 5, which is followed by some concluding remarks in the last section.

2. Briefing of SFEM

A 2D static elasticity problem can be described by equilibrium equation in the problem domain Ω bounded by Γ

$$\sigma_{ij,j} + b_i = 0 \quad \text{in } \Omega \tag{1}$$

which subject to the boundary conditions: $\sigma_{ij}n_j = t_i$ on Γ_t and $u_i = \bar{u}_i$ on Γ_u, where σ_{ij} is the component of stress tensor and b_i the component of body force; n_i is the unit outward normal. Its variational weak form is derived as

$$\int_\Omega \delta \nabla_s(u)_{ij} D_{ijkl} \nabla_s(u)_{kl} \, d\Omega - \int_{\Gamma_t} \delta u_i t_i \, d\Gamma = 0. \tag{2}$$

Similar to FEM, the domain discretization of SFEM is based on element, but the shape of an element can be much more flexible, such as concave element, polygonal and tile element. Galerkin weak form given in Eq. (2) is applied and integration is performed on the basis of element. Depending on the requirement of stability and accuracy, the elements may be further subdivided into finite number of SCs, which is denoted as n_{SC} (see Fig. 1 for example). The issue regarding cell division will be
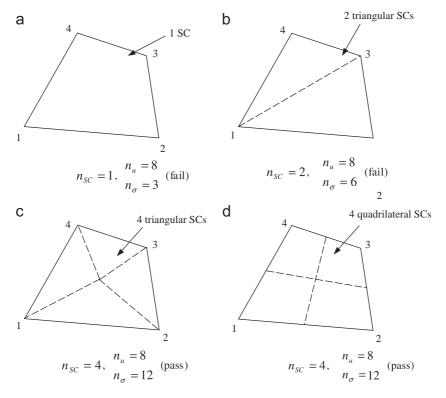

Fig. 1. A free quadrilateral SFEM element with different number of cells for eigenvalue analysis.

studied in more detail in Section 3. Strain smoothing operation and stiffness evaluation are performed simultaneously on each cell. The assembly of stiffness of each cell yields an element stiffness matrix. Detailed formulation can be found in Ref. [3].

In the SFEM, a smoothing operation is performed to the gradient of displacement on the smoothing cell Ω_C, which may be the entire or part of an element

$$\tilde{\nabla} u^h(\mathbf{x}_C) = \frac{\int_{\Omega_C} \nabla u^h(\mathbf{x})\, d\Omega}{\int_{\Omega_C} d\Omega} = \frac{1}{A_C} \int_{\Omega_C} \nabla u^h(\mathbf{x})\, d\Omega, \tag{3}$$

where $A_C = \int_{\Omega_C} d\Omega$ and Ω_C is the smoothing cell. The operation is very similar to the mean dilatation procedure to deal with the incompressibility in nonlinear mechanics [6]. Recently the technique was used by Chen et al. [7,8] to stabilize the nodal integration in the context of mesh-free method.

As in the FEM, upon field discretization, displacement can be approximated by

$$u^h(\mathbf{x}) = \sum_{I=1}^{n} N_I(\mathbf{x}) u_I, \tag{4}$$

where n is the number of nodes in an element. Substituting u^h into Eq. (3) one can get the smoothed gradients of displacement

$$\tilde{\nabla} u^h(\mathbf{x}_C) = \frac{1}{A_C} \int_{\Gamma_C} u^h(\mathbf{x}) \mathbf{n}(\mathbf{x})\, d\Gamma$$

$$= \frac{1}{A_C} \sum_{I}^{n} \int_{\Gamma_C} N_I(\mathbf{x}) \mathbf{n}(\mathbf{x})\, d\Gamma\, u_I, \tag{5}$$

where Γ_C is the boundary of the smoothing cell Ω_C. Note that the smoothing operation makes the domain integration become boundary integration around the smoothing cell in Eq. (5). Particularly in 2D elasticity problems the smoothed strain can be expressed as

$$\tilde{\varepsilon}^h(\mathbf{x}_C) = \sum_{I}^{n} \tilde{\mathbf{B}}_I(\mathbf{x}_C) \mathbf{d}_I, \tag{6}$$

where $\mathbf{d}_I = [u_I \;\; v_I]^T$ is the nodal displacement vector. $\tilde{\mathbf{B}}_I$ is the smoothed strain matrix as

$$\tilde{\mathbf{B}}_I(\mathbf{x}_C) = \begin{bmatrix} \tilde{b}_{I1}(\mathbf{x}_C) & 0 \\ 0 & \tilde{b}_{I2}(\mathbf{x}_C) \\ \tilde{b}_{I2}(\mathbf{x}_C) & \tilde{b}_{I1}(\mathbf{x}_C) \end{bmatrix}. \tag{7}$$

It is easy to relate the smoothed strain matrix $\tilde{\mathbf{B}}_I$ to its counterpart $\mathbf{B}_I = \nabla_s N_I(\mathbf{x})$ in FEM [5] by

$$\tilde{\mathbf{B}}_I = \frac{1}{A_C} \int_{\Omega_C} \mathbf{B}_I(\mathbf{x})\, d\Omega. \tag{8}$$

Therefore, $\tilde{\mathbf{B}}_I$ is the averaged value of the standard $\mathbf{B}_I$ over the cell Ω_C. If one Gaussian point is used for line integration along each edge Γ_i^C of Ω_C, Eq. (7) can be transformed to its algebraic form

$$\tilde{b}_{Ik}(\mathbf{x}_C) = \sum_{i=1}^{M} N_I(\mathbf{x}_i^{GP}) n_{ik}^C l_i^C \quad (k = 1, 2), \tag{9}$$

where $\mathbf{x}_i^{GP}$ is the midpoint (Gaussian point) of boundary segment of Γ_i^C, whose length and outward unit normal are denoted as l_i^C and n_i^C, respectively, and M is the edge number of the cell Ω_C.

The smoothed element stiffness matrix can be obtained by assembly of those on each of the smoothing cell in the element, i.e.,

$$\tilde{\mathbf{K}}_e = \sum_{C}^{n_{SC}} \tilde{\mathbf{B}}_C^T \mathbf{D} \tilde{\mathbf{B}}_C A_C. \tag{10}$$

The smoothed $\tilde{\mathbf{B}}_C$ matrix is constructed on the basis of cell and n_{SC} is the number of cells that the interested element is subdivided.

It is easy to prove that the smoothing operation in a cell ensures that the equilibrium equation is satisfied for each point within the cell and hence it is called equilibrator.

The assemblage of each of the element stiffness matrix $\tilde{\mathbf{K}}_e$ leads to system stiffness matrix and the discrete governing equation is given as

$$\tilde{\mathbf{K}} \mathbf{d} = \mathbf{f}, \tag{11}$$

where $\tilde{\mathbf{K}}$ is the smoothed system stiffness matrix and $\mathbf{f}$ is the nodal force vector given by

$$\mathbf{f}_I = \int_\Omega \mathbf{N}_I^T \mathbf{b}\, d\Omega + \int_\Gamma \mathbf{N}_I^T \mathbf{t}\, d\Gamma. \tag{12}$$

The solution of SFEM using $n_{SC} = 1$ is identical with the FEM using reduced integration. Sometimes the equilibrium model is recovered which secures internal equilibrium and continuous traction transmission [9]. As its stiffness is generally very flexible, the solution corresponds to an upper bound solution. Conversely, if the number of SCs that subdivide an element approaches infinity, one has

$$\tilde{\mathbf{K}}_{IJ} \to \mathbf{K}_{IJ} = \int_\Omega \mathbf{B}_I^T \mathbf{D} \mathbf{B}_J\, d\Omega \quad (\text{as } n_{SC} \to \infty) \tag{13}$$

with n_{SC} approaching infinity, the solution will transform to displacement-compatible model which preserves deformation compatibility over the whole domain including points between adjacent elements. The solution is equivalent to the counterpart in FEM using full integration, which gives a lower bound solution due to the very stiff model. It is proved that for $1 < n_{SC} < \infty$ the solution is not *variationally consistent* [5]. Instead it falls in between the solution of equilibrium model (upper bound) and that of displacement compatible model (lower bound). Since the conformability is only preserved along cell edges and element sides, the generated stiffness matrix of SFEM is not as stiff as the FEM and the computed displacement is generally underestimated and thus more accurate

compared with FEM solution. Instead the loss of conformability inside smoothing cells brings about the equilibrium state of all interior points on them, which gives rise to very good accuracy in both displacement and stress. In addition, besides the comparable convergence rate in displacement, the energy convergence rate in SFEM is proven and numerically observed to be higher than the FEM due to the strain smoothing operation [3,5].

3. Stability condition

As reported in [3] and later on proven in [5], if the entire element is employed as one smoothing cell ($n_{SC} = 1$) zero-energy modes will appear in the eigenvalue analysis of a quadrilateral element. The quadrilateral element divided into four SCs (Fig. 1) can effectively avoid spurious energy modes. Actually further study is still needed to investigate this issue especially for a more general case—a polygonal element.

We first take a free quadrilateral element for example and perform eigenvalue analysis. As shown in Fig. 1, when $n_{SC} = 1$, only three non-zero eigenvalues exist, which is equivalent to three independent "strain relations" ($n_\sigma = 3$) in FEM [1]. When $n_{SC} = 2$ triangular or quadrilateral cells, we can get six

non-zero eigenvalues ($n_\sigma = 6$) but zero-energy modes still exist. When $n_{SC} = 3$ triangular or quadrilateral cells and $n_\sigma = 9$, we find that except three rigid-body-movement modes, no more zero-energy mode appears. Four-triangular and four-quadrilateral cells both work well for this case. For a polygonal element as shown in Fig. 2, it is more natural to divide it into triangular cells. Unless stated otherwise, we mainly use triangular cells for strain smoothing for a polygonal element of arbitrary shape. The next example is standard patch test using a single element of dodecagon shape with three rigid-body movements being fixed. The dodecagonal element is subdivided into different cells as illustrated in Fig. 2. The test results are provided in Table 1. It is seen that, when the number of n_σ is bigger than n_u, single-element patch test can pass, otherwise it will fail, where n_u is the number of displacement freedoms. It is also noticed that for cases of $n_{SC} = 7$ or 8, the patch test passes conditionally. It means that in some cases, patch test can be passed but for others it fails. The general rule is that, for a given number of smoothing cells, the number of edges for each cell should be as small as possible and different types of cells need to be distributed evenly and symmetrically. As such divisions cannot be implemented systematically, they are not recommended in practice.
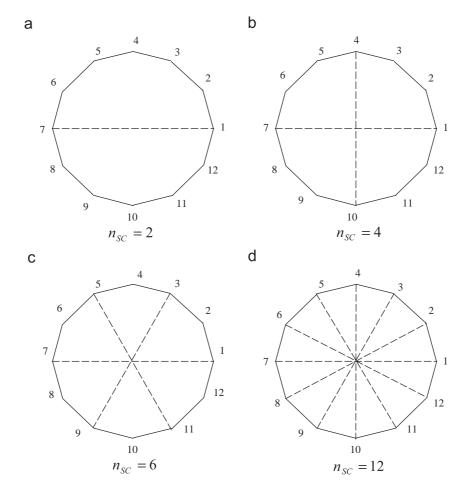

Fig. 2. A dodecagonal SFEM element divided into 2, 4, 6 and 12 smoothing cells subjected to the standard patch test.

Table 1
Division of a dodecagonal element into different number of cells

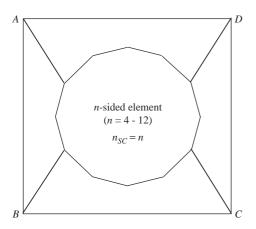| n_u	n_{SC}	$n_\sigma = 3n_{SC}$	$Rank(K_e)$	Patch test	Figure
$n_u = 12 \times 2 - 3 = 21$	2	6	6	Fail	2(a)
	4	12	12	Fail	2(b)
	6	18	18	Fail	2(c)
	7	21	–	Pass (conditionally)	
	8	24	–	Pass (conditionally)	
	12	36	21	Pass (unconditionally)	2(d)

Fig. 3. A patch for the standard patch test with a polygonal element with various number of sides.

A standard patch test is performed for the patch given in Fig. 3 and the number of sides of the central polygonal element is changed from 4 to 12. The element is always subdivided using the same number of cells as its sides. The four corner nodes on the boundary are constrained with a linear displacement field in both directions. It is found that all cases can pass the standard patch test within machine precision without any singularity problems.

Based on these numerical experiments, the following remarks can be made:

(1) One SC is equivalent to one Gaussian quadrature point in FEM with three independent strain relations, which provides three constraints to the cell.
(2) To avoid singularity, a necessary (but not sufficient) condition is that

$$n_\sigma \geqslant n_u, \tag{14}$$

where n_u is the number of the free DOF of displacement and $n_\sigma = 3n_{SC}$ is the number of independent relations of strain or stress.
(3) The number of edges of each smoothing cell should be less than five and different types of cells should be spaced evenly and symmetrically.
(4) The stiffness matrix of an n-sided polygonal element subdivided into n triangular SCs is always non-singular and

hence stable, which is recommended in nSFEM and will be adopted in later examples as well.

4. Selective integration scheme for incompressible material

Volumetric locking tends to appear when the Poisson's ratio approaches 0.5. The application of mixed formulations can avoid such difficulties. A stabilized nodally integrated linear tetrahedral was developed and shown to perform well in problems with nearly incompressible materials [10]. As done in conventional FEM, selective integration is another alternative effective method to deal with this issue, which can also be employed in nSFEM. In FEM different quadrature orders are used for different material parts [11] while in the current method we can simply vary the number of SCs.

The material property matrix $\mathbf{D}$ for isotropic materials can be decomposed as

$$\mathbf{D} = \mathbf{D}_1 + \mathbf{D}_2, \tag{15}$$

where $\mathbf{D}_1$ and $\mathbf{D}_2$ are termed as μ-part and λ-part of $\mathbf{D}$, and the shear modulus $\mu = E/[2(1+v)]$ and $\lambda = vE/[(1+v)(1-2v)]$. The quantities E and v are Young's modulus and Poisson's ratio, respectively. Specifically for plane strain cases

$$\mathbf{D} = \begin{bmatrix} \lambda + 2\mu & \lambda & 0 \\ \lambda & \lambda + 2\mu & 0 \\ 0 & 0 & \mu \end{bmatrix} = \mu \begin{bmatrix} 2 & 0 & 0 \\ 0 & 2 & 0 \\ 0 & 0 & 1 \end{bmatrix}$$

$$+ \lambda \begin{bmatrix} 1 & 1 & 0 \\ 1 & 1 & 0 \\ 0 & 0 & 0 \end{bmatrix} = \mathbf{D}_1 + \mathbf{D}_2. \tag{16}$$

For axisymmetric problems

$$\mathbf{D} = \mu \begin{bmatrix} 2 & 0 & 0 & 0 \\ 0 & 2 & 0 & 0 \\ 0 & 0 & 1 & 0 \\ 0 & 0 & 0 & 2 \end{bmatrix} + \lambda \begin{bmatrix} 1 & 1 & 0 & 1 \\ 1 & 1 & 0 & 1 \\ 0 & 0 & 0 & 0 \\ 1 & 1 & 0 & 1 \end{bmatrix} = \mathbf{D}_1 + \mathbf{D}_2. \tag{17}$$

In nSFEM we use one SC (an entire element) to calculate the stiffness matrix related to λ-part and n SCs to calculate the remainder part, i.e.,

$$\tilde{\mathbf{K}}_e = \tilde{\mathbf{K}}_{e1} + \tilde{\mathbf{K}}_{e2} = \sum_C^n \tilde{\mathbf{B}}_C^T \mathbf{D}_1 \tilde{\mathbf{B}}_C A_C + \tilde{\mathbf{B}}^T \mathbf{D}_2 \tilde{\mathbf{B}} A_e, \tag{18}$$

where A_e is the area of element and n is equal to the number of element sides.

5. Construction of *n*SFEM shape function

In the *n*SFEM, only shape function values at some particular points in an element are needed and no analytical form is required over the entire element. This gives tremendous freedom in shape function construction and many approaches can be used to devise the *n*SFEM shape functions. As stated above, for an *n*-sided polygonal element ($n \geqslant 4$), we can simply divide the element into *n* triangular SCs when calculating element stiffness matrix. The shape functions for the points on an element side are constructed linearly using two related nodes that bound this segment. The shape functions for the interior points can be obtained using the natural element method, polygonal finite elements proposed by Sukumar and Ghosh et al. [12–15], or the

mesh-free techniques, such as MLS/RK methods [16,17], radial point interpolation method (RPIM) [18–21]. It should be mentioned here, mesh-free techniques can be employed to construct shape function for any points, whether on element sides or inside them. Supporting nodes covered in local support domain of the point of interest are used to construct its shape functions. However, similar to the FEM, *n*SFEM only uses nodes of the interested element to derive the shape functions for its interior points in this work. Another point should be stressed that, to maintain geometric conformability between two adjacent elements, linear shape functions are always used on each element side using two related nodes. As problem domain boundaries Γ always coincide with a set of element sides, linear properties can be preserved for shape functions on them. To construct RPIM shape functions with linear polynomial consistency, at least linear polynomial basis should be included in its interpolation basis.
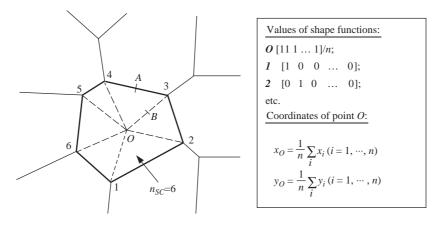

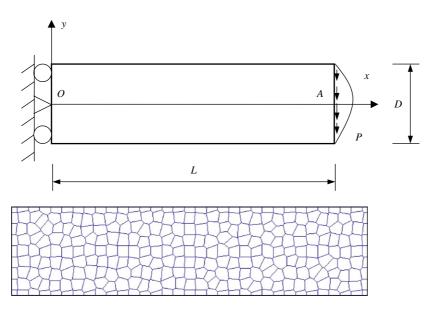Fig. 4. Construction of simple averaging shape functions for a polygonal element.

Fig. 5. Cantilever beam and its polygonal elements using Voronoi diagrams.

For whatever method to be used, the following conditions need to be satisfied for the discrete points of an element: (1) delta function: $N_i(\mathbf{x}_j) = \delta_{ij}$; (2) partition of unity: $\sum_{i=1}^{n} N_i(\mathbf{x}) = 1$; (3) linear compatibility: linear shape functions along element sides; (4) linear consistency: $\sum_{i=1}^{n} N_i(\mathbf{x})\mathbf{x}_i = \mathbf{x}$; and (5) $N_i(\mathbf{x}) \geqslant 0$. Any shape function satisfying the five conditions can be used in SFEM. Condition (4) is essential to reproduce the linear polynomial fields such as in the standard patch test.

A novel and very simple approach is described here to construct a linear displacement field. For a polygonal element, a general central point O can always be found as shown in Fig. 4, whose coordinates are calculated using

$$x_O = \frac{1}{n} \sum_{i}^{n} x_i, \quad y_O = \frac{1}{n} \sum_{i}^{n} y_i, \tag{19}$$

where the number of nodes n of the polygonal element may be different from one element to the other and $\mathbf{x}_i = [x_i \; y_i]^{\mathrm{T}}$.

Due to the linear compatibility property, shape functions at point O can be easily evaluated as

$$O : \left[\frac{1}{n} \; \frac{1}{n} \; \cdots \; \frac{1}{n} \right] \quad (\text{size: } 1 \times n). \tag{20}$$
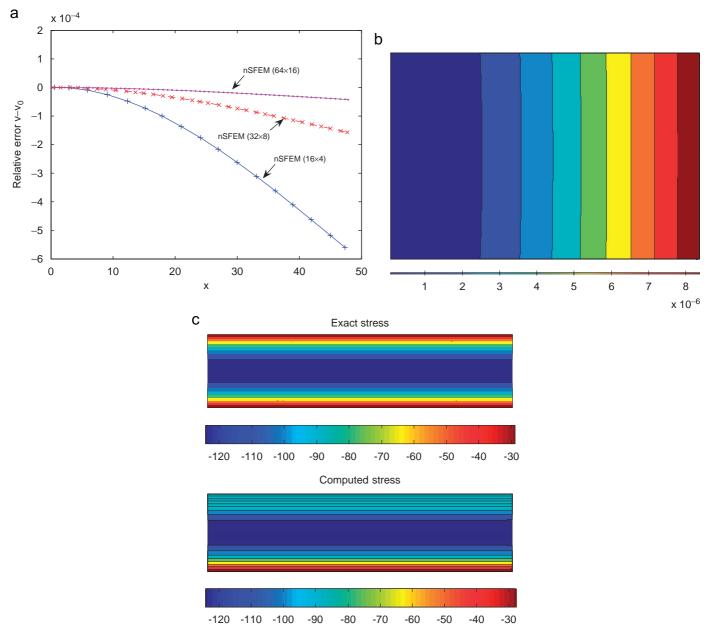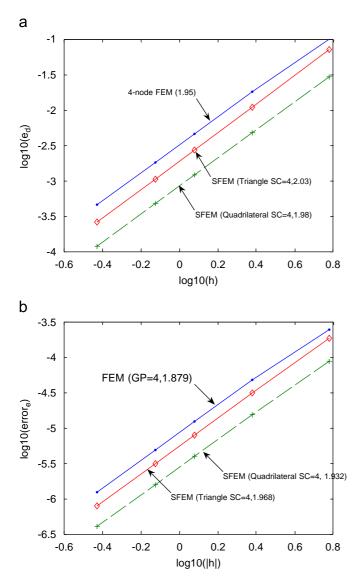

Fig. 6. (a) Relative error of deflection of a cantilever beam; (b) contour plot of relative deflection error and (c) contour plot of exact and computed shear stress τ_{xy}.

a

b

Fig. 7. Convergence rates in: (a) displacement error norm and (b) energy error norm.

Fig. 8. Error in displacement using different Poisson's ratios.

Fig. 9. Infinite plate with a circular hole subjected to unidirectional tension.

It should be mentioned that the purpose of introducing of centroid point O is to facilitate the evaluation of the shape functions of some discrete points inside the interested element. No extra degrees of freedom are associated with point O. In other words, this point carries no additional independent field variable.

When a linear displacement field on a cell edge is used, one Gauss point is sufficient on each edge of a cell (see Fig. 4). Therefore, only shape functions at midpoint on each edge are needed to calculate. For midpoint on the side of the element, its shape functions are evaluated averagely using two related nodes while for interior midpoint, its shape functions are evaluated averagely using point O and the other related node. Using Fig. 4 for example, shape functions at point A are calculated using nodes #3 and #4 while those at B using point O and #3. Nevertheless some special cases may still be encountered in practical computations especially for a concave element.

In order to pass a standard linear patch test, the following points need to be satisfied. If point O coincides with a node, its shape functions should employ the same values as this node
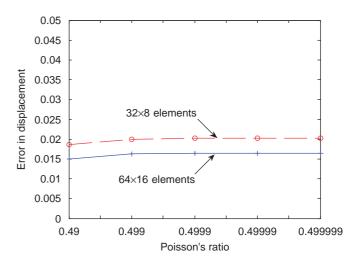
accordingly. If point O is collinear with two nodes of the element, to maintain the linear compatibility property of the shape functions, the shape functions at O now should be constructed linearly using relative distances from the two related nodes. For a smoothing cell with vanishing area, it makes no contribution to the element stiffness matrix. It should be mentioned that, if only convex polygonal elements are used, as to be implemented in the following examples, these cases will never appear.

6. Numerical examples

In this section some examples will be analyzed to demonstrate the effectiveness, accuracy and convergence properties of the present method. The procedure to discretize a problem domain using polygonal elements can be described as follows. The problem domain and it boundaries are first discretized by a set of properly scattered points $\mathbf{P} := \{p_1, p_2, \ldots, p_n\}$. Based on the given points, the domain is further decomposed into the same number of cells $\mathbf{C} := \{c_1, c_2, \ldots, c_n\}$ (i.e., elements in nSFEM), each covering a point such that for any cell, say c_i, all the points in this cell are closer to point p_i
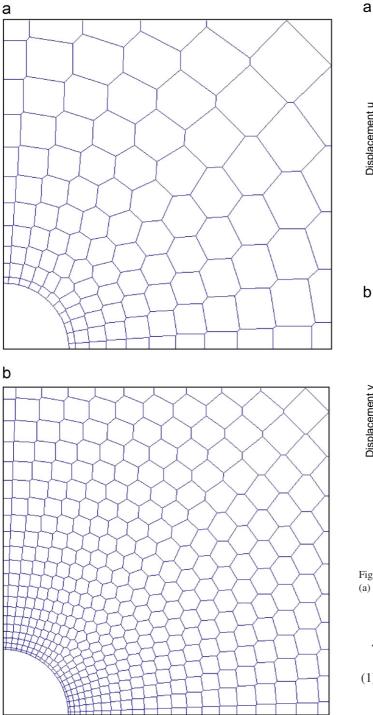
a

b

Fig. 10. Domain discretization of the infinite plate with a hole using: (a) 121 and (b) 441 polygonal elements.

a

b

Fig. 11. Computed and exact displacements of the infinite plate with a hole: (a) u; (b) v.

than they are to any other points $p_j (j \neq i, \ p_j \in \mathbf{P})$ in the domain. The generated regions are the well-known Voronoi diagrams [22]. The initial point p_i is regarded as the *representative point* of the ith element. Voronoi diagrams have a variety of good properties, including convex cells, easy search for nearest neighboring points and largest empty circles, etc. Once we get the information of these Voronoi diagrams, a polygonal element system is founded for numerical analysis.
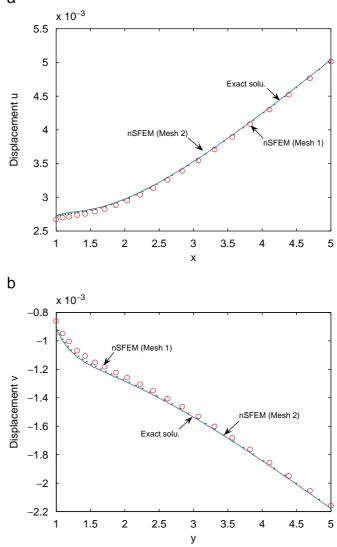
The following points need to be noted:

(1) The original discrete points $\mathbf{P}$ only serve as numerical devices for domain decomposition and do not function in following numerical analysis.

(2) If we prefer more regular elements, such as rectangular elements, hexagon elements, we need to arrange a special point pattern $\mathbf{P}$ before the generation of Voronoi diagrams. For example, in order to obtain rectangular cells in interior domain, initially prescribed points should also be distributed in grid form. Detailed information can be found in mathematical books on this topic.

(3) For demonstration purpose, we arrange the initial points in an arbitrary form in the following examples regardless of the issue of computational cost. As a result, the number of element sides is generally changing from element to element and each is larger than three.
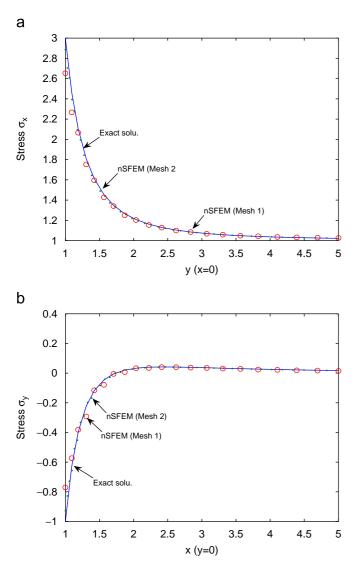
a

b

Fig. 12. Computed and exact stresses of the infinite plate with a hole: (a) σ_x; (b) σ_y.

In the following examples, each element is subdivided into the same number of triangular SCs as its sides (or nodes). If not specified otherwise, the simple averaging shape functions described in Eqs. (19) and (20) are used.

6.1. Cantilever beam

A cantilever beam with length L and height D is studied as benchmark problem, which is subjected to a parabolic traction at the free end as shown in Fig. 5. The beam is assumed to have a unit thickness so that plane stress condition is valid. The analytical solution is available and can be found in a textbook by Timoshenko and Goodier [23].

$$u_1 = \frac{Py}{6EI}\left[(6L - 3x)x + (2+v)\left(y^2 - \frac{D^2}{4}\right)\right],$$

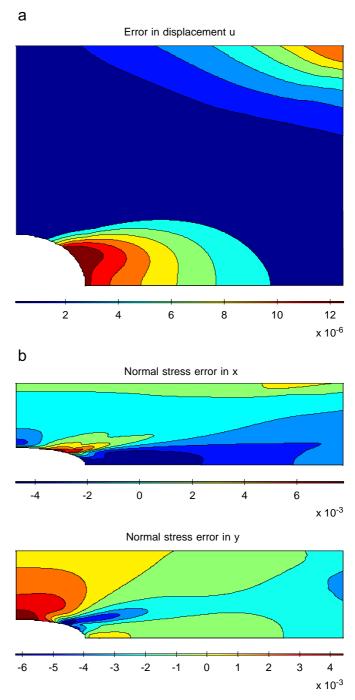$$u_2 = -\frac{P}{6EI}\left[3vy^2(L-x) + (4+5v)\frac{D^2x}{4} + (3L-x)x^2\right]. \quad (21)$$

a

Error in displacement u

b

Normal stress error in x

Normal stress error in y

Fig. 13. Contour plots of: (a) the error in displacement u and (b) the normal stress errors σ_x and σ_y.

where the moment of inertia I of the beam is given by $I = D^3/12$.

The stresses corresponding to the displacements Eq. (21) are

$$\sigma_{11}(x, y) = \frac{P(L-x)y}{I},$$

$$\sigma_{22}(x, y) = 0,$$

$$\tau_{12}(x, y) = -\frac{P}{2I}\left(\frac{D^2}{4} - y^2\right). \quad (22)$$
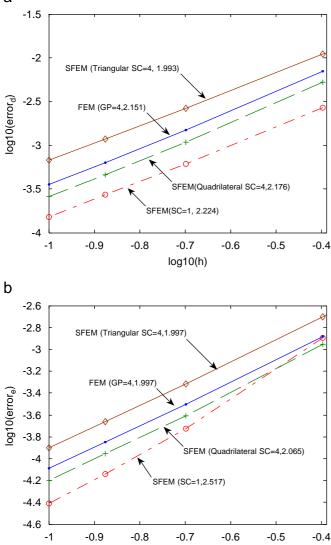
a

b

Fig. 14. Comparison of convergence rates in: (a) displacement norm and (b) energy norm.

The related parameters are taken as $E = 3.0 \times 10^7$ kPa, $v = 0.3$, $D = 12$ m, $L = 48$ m and $P = 1000$ N.

In order to study the convergence rate of the present method, two norms are used here, i.e., displacement norm and energy norm, as defined by

$$e_{\mathrm{d}} = \frac{\sum |u_i - u_i^h|}{\sum |u_i|},$$

$$e_{\mathrm{e}} = \frac{1}{2LD} \left[\int_{\Omega} (\boldsymbol{\varepsilon}^h - \boldsymbol{\varepsilon})^{\mathrm{T}} \mathbf{D} (\boldsymbol{\varepsilon}^h - \boldsymbol{\varepsilon}) \right]^{1/2}. \qquad (23)$$

In the computations, the nodes on the left boundary are constrained using the exact displacements obtained from Eq. (21) and the loading on the right boundary uses the exact distributed parabolic shear stresses in Eq. (22). The beam is analyzed using different number of elements. Fig. 5 gives one example for the discretization of the beam. The relative deflection along $y = 0$ and the contour of relative deflection errors and the
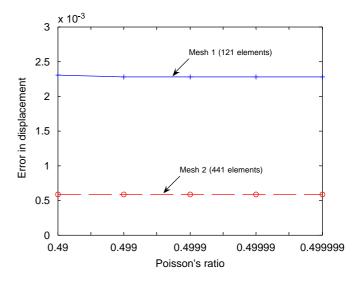

Fig. 15. Error in displacement using different Poisson's ratios.

exact and computed shear stress τ_{12} are demonstrated in Fig. 6. It is seen very accurate results are obtained as compared with exact solutions. It is observed that, similar to the conventional FEM results, the computed displacement is underestimated and approaches the exact solution with the increase of elements for this case. Due to the smoothing techniques, the computed strains/stresses are constant within every SC and each has a set of values. When computing stresses of an element, we can average all sets of stresses on all the SCs in the element and regard them as the stresses of the centroid point O (Fig. 4). The point O is used as representative stress point of the element. The stresses preferably have to be weighted using the respective area of each cell. The convergence rates in displacement and energy are demonstrated in Fig. 7. For easy and fair comparison, we now use regular quadrilateral elements, each subdivided into four triangular or quadrilateral cells for integration. In the four-node FEM 2×2 Gauss points in an element are used for computing displacements and one Gauss point for computing stresses and energy. So the full superconvergence with optimal error $O(h^2)$ can be obtained for FEM [1]. It is observed from this figure that both nSFEM and FEM give largely comparable convergence rates in displacement and energy. The results using nSFEM are more accurate than the FEM. In nSFEM, quadrilateral cell seems to perform better than triangular cell.

To investigate the capability of nSFEM in solving problems involving nearly incompressible materials, two polygonal meshes are employed with Poisson's ratio approaching 0.5 gradually. The selective integration described in Section 4 is used. It is noticed from Fig. 8 that the method works very well for this kind of material (plane strain problem). When Poisson's ratio is bigger than 0.499, the error in displacement almost remains constant.

6.2. Infinite plate with a circular hole

Fig. 9 represents a plate with a central circular hole subjected to a unidirectional tensile load of 1.0 N/m at infinity in the

x-direction and Fig. 10 gives the discretization of the domain using two kinds of meshes (121 and 441 elements). Due to its symmetry, only the upper right quadrant of the plate is modeled. Plane strain condition is considered and $E = 1.0 \times 10^3 \, \text{N/m}^2$, $v = 0.3$. Symmetry conditions are imposed on the left and bottom edges, and the inner boundary of the hole is traction free. The exact solution for the stresses is [23]

$$\sigma_{11} = 1 - \frac{a^2}{r^2}\left[\frac{3}{2}\cos 2\theta + \cos 4\theta\right] + \frac{3a^4}{2r^4}\cos 4\theta,$$

$$\sigma_{22} = -\frac{a^2}{r^2}\left[\frac{1}{2}\cos 2\theta - \cos 4\theta\right] - \frac{3a^4}{2r^4}\cos 4\theta,$$

$$\tau_{12} = -\frac{a^2}{r^2}\left[\frac{1}{2}\sin 2\theta + \sin 4\theta\right] + \frac{3a^4}{2r^4}\sin 4\theta, \tag{24}$$

where (r, θ) are the polar coordinates and θ is measured counterclockwise from the positive x-axis. Traction boundary conditions are imposed on the right ($x = 5$) and top ($y = 5$) edges based on the exact solution Eq. (24). The displacement components corresponding to the stresses are

$$u_1 = \frac{a}{8\mu}\left[\frac{r}{a}(\kappa + 1)\cos\theta + 2\frac{a}{r}((1 + \kappa)\cos\theta + \cos 3\theta)\right.$$
$$\left. -2\frac{a^3}{r^3}\cos 3\theta\right],$$

$$u_2 = \frac{a}{8\mu}\left[\frac{r}{a}(\kappa - 1)\sin\theta + 2\frac{a}{r}((1 - \kappa)\sin\theta + \sin 3\theta)\right.$$
$$\left. -2\frac{a^3}{r^3}\sin 3\theta\right], \tag{25}$$

where κ is defined in terms of Poisson's ratio by $\kappa = 3 - 4v$ for plane strain cases.

From Figs. 11 and 12, it is observed that all the computed displacements and stresses are in good agreement with the analytical solutions. With the refinement of the mesh, the accuracy is getting better. It is also noticed that the present stresses are very smooth though no post-processing is performed for them. The contour plots of the error in displacement and stresses are displayed in Fig. 13. Very good accuracy can be obtained. The convergence rates in displacement and energy are demonstrated in Fig. 14 using quadrilateral elements for both FEM and nSFEM. The simple method described in Eq. (20) is employed to form the nSFEM shape functions. It is seen that the nSFEM using four quadrilateral cells gives much more accurate results and higher convergence rates in displacement and energy than using triangular cells and FEM results. When using nSFEM with triangular cells, if RPIM method with linear polynomial reproduction is used to construct the shape function for interior points of an element, the accuracy for both displacement and energy can be improved greatly. Fig. 15 shows the error in displacement for nearly incompressible material using two polygonal meshes. Once again the error seems constant with the increase of Poisson's ratio.

6.3. Connecting bar

The last example performs a static analysis of an automobile part, a connecting bar with a relatively complex configuration, as shown in Fig. 16. The boundary conditions as well as the applied load are demonstrated in this figure with $p = 1 \, \text{MPa}$. Two types of meshes are used for analysis with 346 elements in
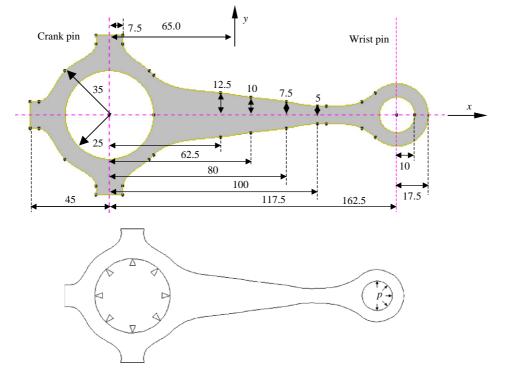

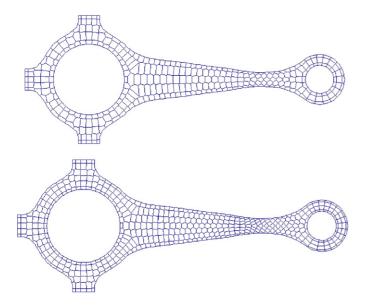Fig. 16. Geometric model and boundary conditions an automobile connecting bar.

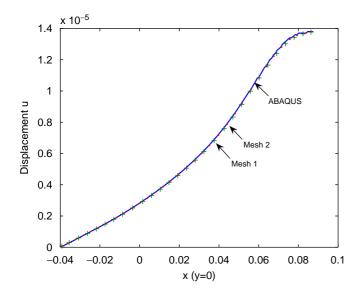Fig. 17. Domain discretization of the connecting bar using two meshes (346 and 525 polygonal elements).

Fig. 19. Normal stress σ_x from the present method and FEM via ABAQUS.

Fig. 18. Displacement u from the present method and FEM via ABAQUS.

mesh 1 and 525 in mesh 2 as illustrated in Fig. 17. Plane stress problem is considered with material constants $E = 10$ GPa and $v = 0.3$. As no closed form solutions are available, a reference solution is obtained using the commercial software ABAQUS® with 10364 nodes. Fig. 18 gives the displacement distributions along x-axis and it is observed that they are in good accord as compared with the ABAQUS solutions. The coarse mesh still gives satisfactory displacements. Fig. 19 demonstrates the stress distributions along the x- axis. It is noticed again that the stresses are very smooth as the previous example. Very good agreement is seen except those close to the boundary nodes. Increasing the number of elements near boundary can enhance the accuracy.
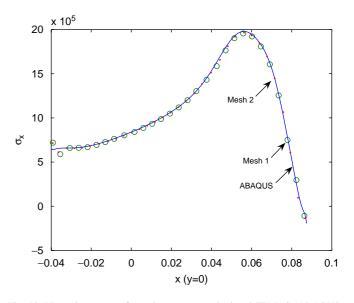
7. Concluding remarks

Smoothed finite element method (SFEM) was recently proposed to improve the accuracy and convergence rate of the conventional four-node isoparametric finite elements. Due to the introducing of strain smoothing procedure the coordinate transformation is not necessary and thus the restriction on the shape of quadrilateral elements can be eliminated for mapped elements. In this work SFEM has been extended to more general case, an n-sided polygonal element (or nSFEM), and problem domain can be discretized in a very flexible manner.

The stability analysis is performed for polygonal elements and it is found that one SC is equivalent to one quadrature point in FEM, which provides three independent strain relations (or constraints). A criterion is provided to determine the proper number of cells that an element is subdivided. A polygonal element subdivided into the same number of triangular cells as its sides is always stable and gives good accuracy in computations. Selective integration scheme is recommended for solving volumetric locking problems concerning nearly incompressible materials.

Several numerical experiments are analyzed and it is found that the present method obtains very accurate results with the employment of the simple shape function described in the work. The computed displacement can be improved by using other higher order shape functions such as MLS/RPIM. It should be mentioned that, it may not be wise to use polygonal elements all along in the entire problem domain as enlarged number of nodes will increase the computational cost but not reduce the dimension of elements or enhance the convergence property prominently. However, our suggestion is that for interior region of a problem domain, four-node quadrilateral smoothed elements are strongly recommended but polygonal elements can be used for region near boundary or very irregular parts. In addition, it is very straightforward and convenient to integrate the technique with the conventional finite elements when

necessary, such as problems with complicated configuration. Though only 2D linear elasticity problems are investigated in this work, there is no difficulty to apply *n*SFEM to some other more complicated cases, such as 3D problems, time-dependent transient problems or those involving material and geometric nonlinearities.

References

[1] O.C. Zienkiewicz, R.L. Taylor, The Finite Element Method, fifth ed., Butterworth Heinemann, Oxford, 2000.

[2] G.R. Liu, S.S. Quek, The Finite Element Method: a Practical Course, Butterworth Heinemann, Oxford, 2003.

[3] G.R. Liu, K.Y. Dai, T.T. Nguyen, A smoothed finite element method for mechanics problems, Comput. Mech. 39 (2007) 859–877.

[4] K.Y. Dai, G.R. Liu, Free and forced vibration analysis using the smoothed finite element method (SFEM), J. Sound Vib. 301 (2007) 803–820.

[5] G.R. Liu, T.T. Nguyen, K.Y. Dai, K.Y. Lam, Theoretical aspects of the smoothed finite element method (SFEM), Int. J. Numer. Methods Eng. (2006) in press.

[6] J. Bonet, R.D. Wood, Nonlinear Continuum Mechanics for Finite Element Analysis, Cambridge University Press, Cambridge, 1997.

[7] J.S. Chen, C.T. Wu, S. Yoon, Y. You, A stabilized conforming nodal integration for Galerkin meshfree method, Int. J. Numer. Methods Eng. 50 (2001) 435–466.

[8] J.S. Chen, C.T. Wu, T. Belytschko, Regularization of material instabilities by meshfree approximations with intrinsic length scales, Int. J. Numer. Methods Eng. 47 (2000) 1303–1322.

[9] D.W. Kelly, Reduced integration to give equilibrium models for assessing the accuracy of finite element analysis. Proceedings of Third International Conference Australia Finite Elem. Meth., July, 1979.

[10] M.A. Puso, J. Solberg, A stabilized nodally integrated tetrahedral, Int. J. Numer. Methods Eng. 67 (2006) 841–867.

[11] T.J.R. Hughes, The Finite Element Method: linear Static and Dynamic Finite Element Analysis, Prentice-Hall, 1987.

[12] N. Sukumar, Construction of polygonal interpolants: a maximum entropy approach, Int. J. Numer. Methods Eng. 61 (2004) 2159–2181.

[13] N. Sukumar, B. Moran, T. Belytschko, The natural element method in solid mechanics, Int. J. Numer. Methods Eng. 43 (1998) 839–887.

[14] S. Ghosh, Y.S. Liu, Voronoi cell finite element model-based on micropolar theory of thermoelasticity for heterogeneous materials, Int. J. Numer. Methods Eng. 38 (1995) 1361–1398.

[15] S. Ghosh, S. Moorthy, Elastic-plastic analysis of arbitrary heterogeneous materials with the Voronoi-cell finite element method, Comput. Meth. Appl. Mech. Eng. 121 (1995) 373–409.

[16] T. Belytschko, Y.Y. Lu, L. Gu, Element-free Galerkin methods, Int. J. Numer. Methods Eng. 37 (1994) 229–256.

[17] W.K. Liu, S. Jun, Y.F. Zhang, Reproducing kernel particle methods, Int. J. Numer. Methods Eng. 20 (1995) 1081–1106.

[18] G.R. Liu, Mesh-free Methods: Moving Beyond the Finite Element Method, CRC Press, Boca Raton, FL, 2002.

[19] J.G. Wang, G.R. Liu, A point interpolation meshless method based on radial basis functions, Int. J. Numer. Methods Eng. 54 (2002) 1623–1648.

[20] K.Y. Dai, G.R. Liu, K.M. Lim, Y.T. Gu, Comparison between the radial point interpolation and the Kriging based interpolation used in mesh-free methods, Comput. Mech. 32 (2003) 60–70.

[21] K.Y. Dai, G.R. Liu, K.M. Lim, X. Han, S.Y. Du, A meshfree point interpolation method for analysis of functionally graded material (FGM) plates, Comput. Mech. 34 (2004) 213–223.

[22] A. Okabe, B. Boots, K. Sugihara, Spatial Tessellations: Concepts and Applications of Voronoi Diagrams, Wiley, Chichester, 1992.

[23] S.P. Timoshenko, J.N. Goodier, Theory of Elasticity, third ed., McGraw-Hill, New York, NY, 1970.